coatings

MDPI

Article

The Effect of In Situ Laser-Assisted Plasma Spraying on the Plasma Etching Resistance of Yttrium Oxide Coating

Xutao Zhao [1,2,3], Tian Xie [1,3], Panpan Zhang [1,3], Zhehe Yao [1,3], Qunli Zhang [1,3], Jiake Deng [4], Yongfeng Sui [5] and Jianhua Yao [1,3,*]

[1] College of Mechanical Engineering, Zhejiang University of Technology, Hangzhou 310023, China; zxt1987@usx.edu.cn (X.Z.); shaoxingwenlilaser@163.com (T.X.); panpanzhang166@163.com (P.Z.); zhyao@zjut.edu.cn (Z.Y.); zql@zjut.edu.cn (Q.Z.)
[2] School of Mechanical and Electrical Engineering, Shaoxing University, Shaoxing 312000, China
[3] Institute of Laser Advanced Manufacturing, Zhejiang University of Technology, Hangzhou 310023, China
[4] Wuhan HGLaser Engineering Co., Ltd., Wuhan 430070, China; djk@hglaser.com
[5] Hangzhou Turbine Power Group Co., Ltd., Hangzhou 310015, China; zivt1989@163.com
* Correspondence: lam@zjut.edu.cn

Abstract: In recent years, yttrium oxide coatings prepared by atmospheric plasma spraying (APS) have been employed extensively in semiconductor processing equipment. Meanwhile, defects in yttrium oxide coating, such as unmelted particles and pores, reduce the etching resistance of the coating. In this work, two yttrium oxide coatings were prepared by in situ laser-assisted plasma spraying (LAPS) coupled with a 500 W and 600 W laser for comparison with a coating prepared by APS, and the effects of the laser on the coating properties were investigated. The results show that the surface roughness was reduced by 25.7% (500 W) and 25.3% (600 W) and the porosity was reduced by 52.3% (500 W) and 36.9% (600 W) after laser coupling. After being etched by CF_4/CHF_3 for a long time, it was observed from SEM, EDS and XPS analyses that the intensity ratios of the Y-F bonds in the coating were 1 (APS):1.3 (LAPS+500W):1.1 (LAPS+600W), which indicated that the LAPS+500W coating had a thicker fluorination layer. It was also observed that the fluorination layer at the defect was first eroded; then, the erosion area gradually spread to the surrounding area, and finally, the fluorination layer was etched. This indicated that the defects had a significant impact on the etching resistance. Consequently, the LAPS+500W coating with fewer defects and a thicker fluorination layer showed the lowest etching rate. Therefore, in situ laser-assisted plasma spraying coupled with an appropriate laser power is an effective method to improve the performance of yttrium oxide coatings.

Keywords: APS; LAPS; Y_2O_3; plasma etching; fluorination

Citation: Zhao, X.; Xie, T.; Zhang, P.; Yao, Z.; Zhang, Q.; Deng, J.; Sui, Y.; Yao, J. The Effect of In Situ Laser-Assisted Plasma Spraying on the Plasma Etching Resistance of Yttrium Oxide Coating. *Coatings* **2024**, *14*, 1427. https://doi.org/10.3390/coatings14111427

Academic Editor: Alessandro Patelli

Received: 7 October 2024
Revised: 1 November 2024
Accepted: 4 November 2024
Published: 10 November 2024

1. Introduction

With the continuous reduction in chip processing size, high-density plasma etching technology faces many challenges, one of which is the problem of particle contamination. During the etching process, ceramic components such as electrodes, shower heads, gaskets and focusing rings react with plasma and are corroded [1–3]. Due to the large contact area and long exposure time of the inner wall of the processing chamber cavity, the aforementioned problems can be much more serious. Aluminum alloy has become the main material in machining chambers due to its considerable vacuum performance. However, aluminum alloy is very susceptible to corrosion by fluorinated plasma. Due to the strong etching ability of silicon-based materials, plasma etching gases are mainly fluorinated gases, such as CF_4, CF_4/CHF_3, C_2F_6, SF_6 and NF_3. CF_4/CHF_3 gas is widely used, and the process is versatile, so it can cover most existing chip manufacturing processes, but it does not perform well on hard materials. Therefore, a protective coating is needed to improve its resistance to plasma corrosion [4–7]. Early protective coatings were composed

of silicon-based materials (SiO_2 and SiC), and subsequently, aluminum oxide (Al_2O_3) replaced silicon-based materials due to its better etching resistance. With the development of chip manufacturing technology, yttrium oxide superseded aluminum oxide in terms of its better chemical stability and corrosion resistance [8–10]. In recent years, some scholars have explored new coating materials such as YOF and YF_3 or added zirconia to yttrium oxide to improve their performance, but yttrium oxide is still the mainstream cavity coating material from the perspectives of cost and process [11–16].

The principal preparation methods of yttrium oxide coatings are atmospheric plasma spraying (APS), suspended plasma spraying (SPS) and aerosol deposition (AD), but considering the production cost and technical barriers, APS is the most suitable method [17–19]. APS is generally performed with agglomerated sintered powder with a particle size of 30 μm. During the deposition process, impact fractures and nonmelting will occur, leading to the formation of internal defects such as pores and cracks, which will have a detrimental impact on the quality of the coating. This has drawn the attention of many scholars. Minjoong Kim et al. [20] investigated the APS coating microstructure of yttrium oxide powders with different particle sizes and found that powders with small particle sizes can form high-density coatings and improve the etching resistance. L. Dubourg et al. [21] used laser para-assisted plasma spraying to prepare an alumina-titanium dioxide coating and found that when the laser energy density was between 15 and 22 W/mm^2, the cracks and pores in the coating were greatly reduced, and the erosion resistance was improved. Zhou et al. [22] found that after laser remelting, the particles of AT13 composite ceramic coating were refined, the lamellar structure disappeared, and the density increased. The bond strength, microhardness, wear resistance, erosion resistance and thermal shock performance were significantly improved. Chong et al. [23] used the pulsed laser technique to remelt Cr_3C_2-NiCr coatings prepared by supersonic spraying and found that the porosity was reduced by 74% and the carbide volume fraction increased by 42.9%, the coating microstructure was more homogeneous and denser, and the hardness and corrosion resistance were greatly improved after laser remelting. Janka et al. [24] argued that the heat input of the laser at a low power would not remelt the Cr_3C_2-NiCr coating. Compared with the as-sprayed coating, the microstructure and the distribution of carbides did not change, but there were more secondary chromium carbides. Our team combined LAPS and APS to prepare a molybdenum coating and found that the coating porosity could be controlled by adjusting the laser power and the best-performing coating can be obtained with a laser power of 500 W [25].

Therefore, laser-assisted plasma spraying is an effect method to improve the coating performance, but to date, most research has focused on laser remelting; in situ laser irradiation-modified plasma spraying has rarely been studied. However, in situ laser-assisted plasma spraying can be more accurate in terms of the microstructure and tissue distribution control of the coating by regulating the laser power. Especially for ceramic coatings, it can effectively alleviate defects such as cracks generated during laser remelting. In this study, yttrium oxide coatings prepared by in situ laser-assisted atmospheric plasma spraying and APS were compared. The effects of the laser power on the interfacial structure and porosity of the yttrium oxide coating applied by plasma spraying were studied. The relationship between the yttrium oxide coating density and etching performance was also discussed.

2. Materials and Methods

The substrate was aluminum alloy (Al6061-T6) and the chemical composition (wt%) of the Al6061-T6 is listed as follows: 0.393 Si, 0.246 Gu, 0.96 Mg, 0.001 Zn, 0.086 Mn, 0.015 Ti, 0.05 Gr, 0.462 Fe, and 97.8 Al. The substrate was machined into a 20 mm × 20 mm × 5 mm block. The material was Yttrium oxide with a particle size ranging from 15 to 50 μm with the average size of 40 μm and purity ≥ 99.9% (Shanghai Xiangtian Nanomaterials Co., Ltd., Shanghai, China). The experimental device for the LAPS process was constituted by the coupling of an atmospheric plasma spray gun (XM-SG100, Xiuma Spraying Machincry,

Shanghai, China) and a 6 KW semiconductor laser (LDF6.000-40VGP, Laserline, Koblenz, Germany) with a wavelength of 940 nm, as shown in Figure 1a. The laser was at a 60° angle to the substrate. The plasma gun and semiconductor laser were connected by a fixture to ensure consistent action during the spraying process. The diameter of the laser spot was 6 mm. Before depositing, the aluminum alloy substrate was ultrasonically cleaned with anhydrous alcohol, and then sandblasted. After sandblasting, the residual sand and gravel were blown away with high-pressure nitrogen. The preparation method of the coatings in this experiment was as follows: the center of the laser spot and the spray gun powder spot coincided, and the laser was irradiated on the deposited particles synchronously. Three kinds of coatings were prepared with the same process parameters except for the laser power, as shown in Table 1.

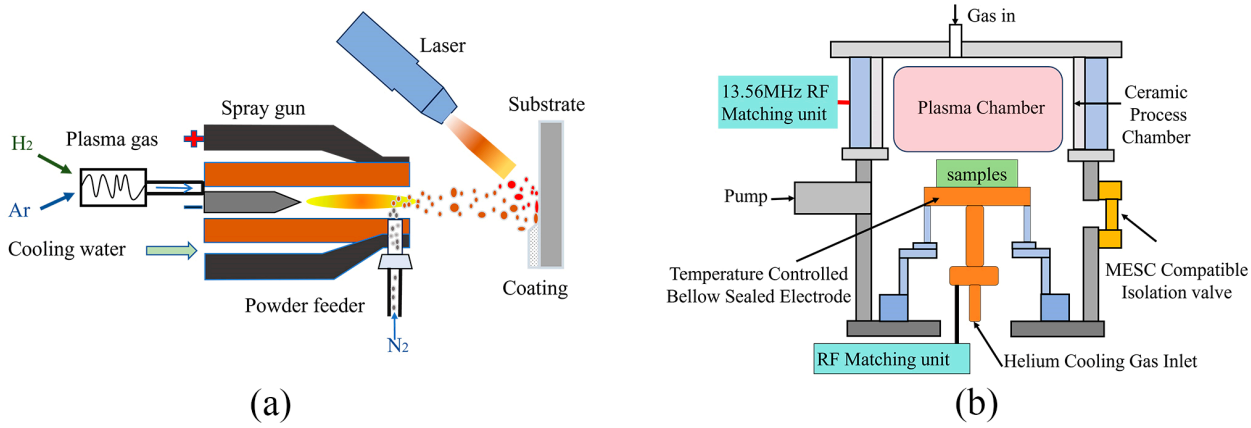

Figure 1. Schematic diagram of (**a**) in situ laser-assisted plasma spraying and (**b**) system for CF_4/CHF_3 plasma etching.

Table 1. Parameters of in situ laser-assisted plasma spraying process.

No.	Current (A)	Voltage (V)	Primary Gas, Ar (SLPM)	Primary Gas, H_2 (SLPM)	Spray Distance (mm)	Powder Feed Rate (g/min)	Gun Speed (mm/min)	Overlap Distance (mm)	Laser Power (W)
1	700	58	45	3	100	15	100	4	0
2	700	58	45	3	100	15	100	4	500
3	700	58	45	3	100	15	100	4	600

The samples were cut and embedded in epoxy resin (the cross-sections of coatings were exposed), polished and then observed. In the process, standard metallographic methods were followed. Image J ver.1.8.0.345 analysis software was used to analyze the porosities of the entire cross-section of the coatings. The surface roughness of the coatings was measured using a confocal laser microscope (VK-X1100, KEYENCE, Osaka, Japan). Inductively coupled plasma etcher (GSEC200, NAURA, Beijing, China) was used for plasma etching, as shown in Figure 1b. The Ar, CF_4 and CHF_3 gases in the chamber were mixed at a ratio of 1:1:4. SRF (Source Radio Frequency) was used to generate plasma (1800 W, 1–2 min), and then BRF (Bias Radio Frequency) was used for plasma etching (200 W, 20 min). After the etching was completed, O_2+SF_6 gases were applied for cleaning (10 min), and this procedure was repeated 220 times. The microstructures of the samples were studied with a field emission electron microscope (FE-SEM, Sigma 300, Zeiss, Oberkochen, Germany) equipped with an energy-dispersive spectroscope (EDS). Phase compositions were determined using an X-ray diffractometer (XRD, Empyrean, Almelo, Holland). The element binding states of the Y_2O_3 coatings were characterized by X-ray photoelectron spectroscopy (XPS, ESCALAB 250Xi, Waltham, MA, USA) with a monochromated Al Kα source.

3. Results and Discussion

3.1. Cross-Sectional Analysis

In the conventional thermal spraying process, the time for powder particles to absorb heat is a fixed parameter. As the particle size decreases, the ease of melting and deposition in the form of droplets increase. However, due to insufficient heat absorption, large-scale particles can only be deposited in an unmelted state, resulting in fragmentation and splashing, which increases the internal defects of the coating [24–27]. Figure 2a–d illustrate the electron microscope cross-section images of the yttrium oxide coatings deposited by APS and LAPS coupled to a 500 W and 600 W laser, respectively. The defects observed in the coatings were pores and cracks. The primary defects of the APS (Figure 2a) and LAPS+500W (Figure 2b) coatings were pores, whereas the LAPS+600W coating exhibited pronounced transverse and longitudinal cracks (Figure 2d). The porosity of the LAPS coatings is shown in Table 2.

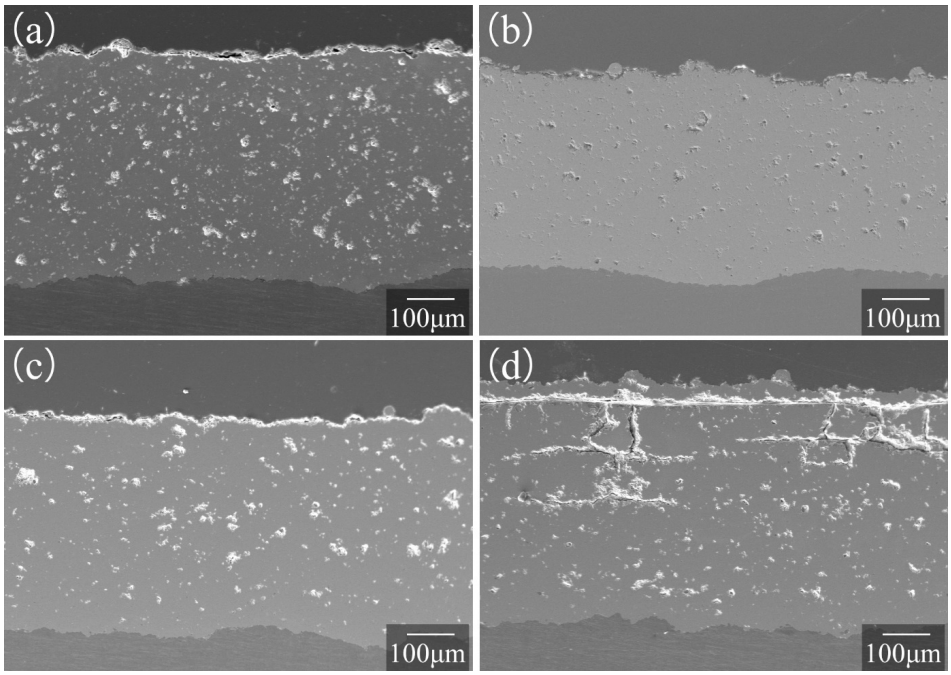

Figure 2. FE-SEM images of cross-sectional of Y_2O_3 coatings: (**a**) APS; (**b**) LAPS+500W; (**c**) LAPS+600W; (**d**) LAPS+600W with cracks.

Table 2. Porosity and roughness of LAPS coatings with different laser powers.

	APS	LAPS+500W	LAPS+600W
Laser power (W)	0	500	600
Porosity	7.84%	3.74%	4.95%
Roughness (μm)	12.941	9.61	9.671

The APS coating exhibited a considerable number of unmelted particles and pores, some of which were contiguous. This is a typical phenomenon of insufficient heat input, and the unmelted particles in the pores were mainly mechanical bonds or semi-mechanical semi-metallurgical bonds, which would reduce the cohesion of the coating. The LAPS+500W coating showed a higher density and a smaller thickness. This was because the introduction of the laser resulted in an increased heat input during the deposition process, which in turn led to a greater number of particles being deposited in a molten or semi-molten state. As a result, the number and size of the large pores were reduced, most of the fine pores were sealed, and the connected pores disappeared. The defects in the LAPS+600W coating showed that a higher laser power would result in an excessive heat input. The

significant temperature differential during the rapid cooling process led to the generation of considerable thermal stress, ultimately causing the formation of cracks. Meanwhile, the coating surrounding the crack was relatively dense, thereby maintaining the overall porosity of the coating within a specified range. As the number of deposited particles increased, the coating thickness also increased. Despite the elevated heat input resulting from the laser coupling, the coating did not undergo remelting.

Figure 3 shows the XRD patterns of the three coatings. It can be observed that the diffraction peaks of the three coatings remained unaltered, and that the intensity of the peaks were essentially consistent. No new phases appeared during the crystallization process, and no impurities were produced. This indicated that the laser coupling does not change the crystallization process of yttrium oxide.

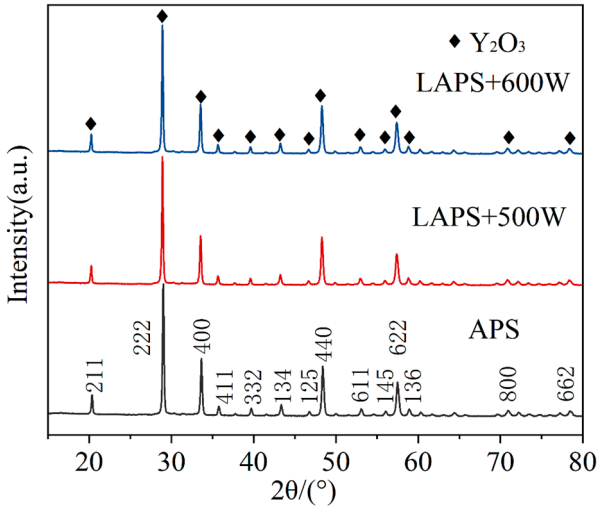

Figure 3. XRD patterns of APS, LAPS+500W, LAPS+600W.

3.2. Surface Topography Analysis

The roughness of the LAPS coatings is shown in Table 2. It shows that the roughness of the LAPS+500W and LAPS+600W coatings was reduced by 25.7% and 25.3%, respectively, in comparison to the APS coating. Figure 4 shows the 3D images of about 0.9 cm^2 of the central area of the surface of three coatings. The APS coating was thicker in the middle and thinner on both sides, which is a typical thermal spraying coating topography (Figure 4a).

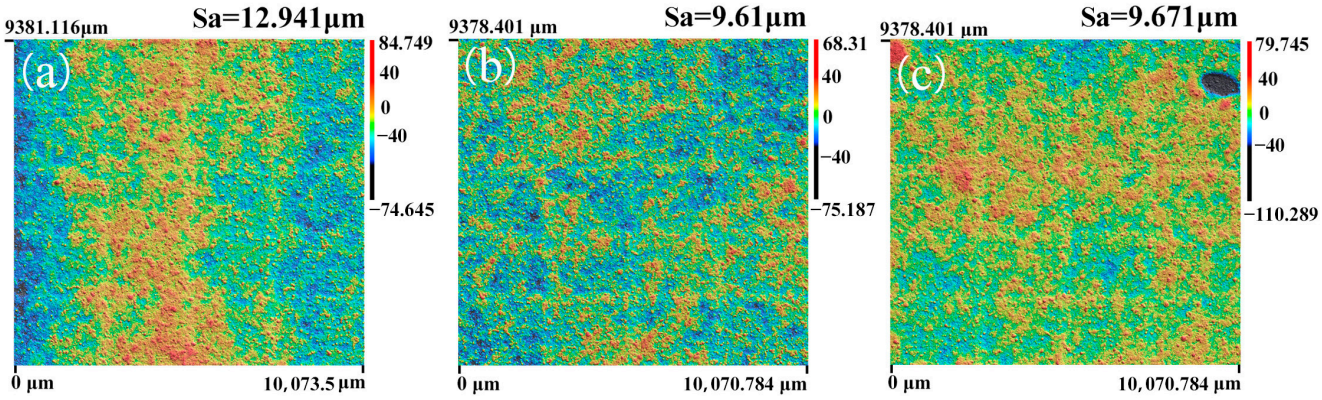

Figure 4. The roughness of projected coatings: (**a**) APS; (**b**) LAPS+500W; (**c**) LAPS+600W.

In contrast, the LAPS coatings exhibited a relatively uniform surface with no discernible peaks or valleys (Figure 4b,c). This phenomenon might be attributed to the flow of particles that have melted, which was reflected in the surface roughness.

Figure 5a shows the surface morphology of the three coatings. The LAPS+500W coating rarely had large unmelted particles; this was consistent with the cross-section morphology shown in Figure 2b. As a result, the coating had a lower roughness and a smoother surface while the rough microstructure could reduce the performance of the coating in plasma etching. Figure 5b shows the surface morphology of the three coatings following exposure to CF_4/CHF_3 plasma etching. It shows that the numerous pores were exposed and the large unmelted particles deposited on the surface were bombarded out of the cracks, rendering the coating more susceptible to corrosion. Among the three coatings, the LAPS+500W coating had the smoothest morphology and fewest defects. This could be attributed to the superior quality of the original coating, the fewer defects and the formation of a relatively uniform fluorination layer subsequent to etching.

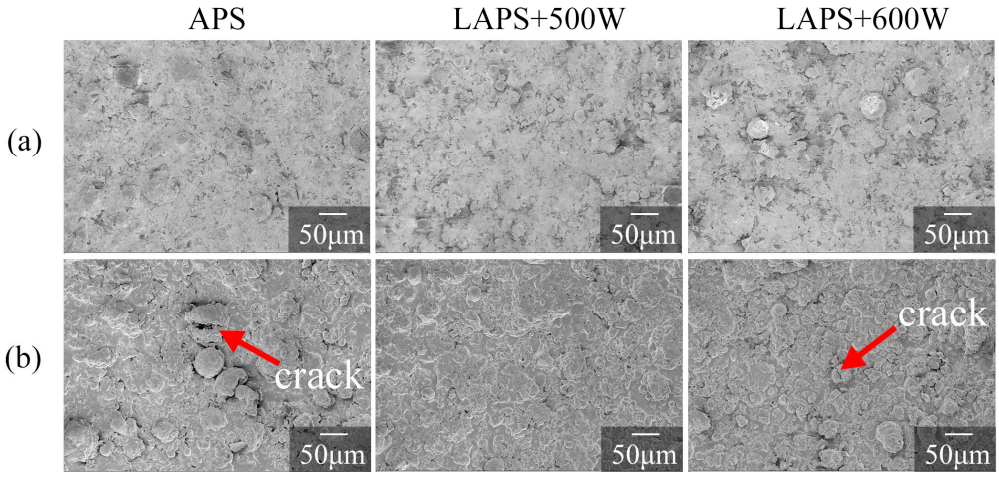

Figure 5. FE-SEM images of coating surfaces (**a**) before and (**b**) after CF_4/CHF_3 etching.

As can be seen from the EDS maps of the coating surfaces (Figure 6), fluorine appeared in all three coatings following plasma etching, and its distribution was predominantly observed at the boundary of the yttrium and oxygen elements [20]. However, in the LAPS+500W coating, some fluorine was observed to overlap with the yttrium and oxygen elements. The presence of fluorine indicated the formation of a fluorination layer, and the coincidence degree reflected the uniformity of the fluorination layer.

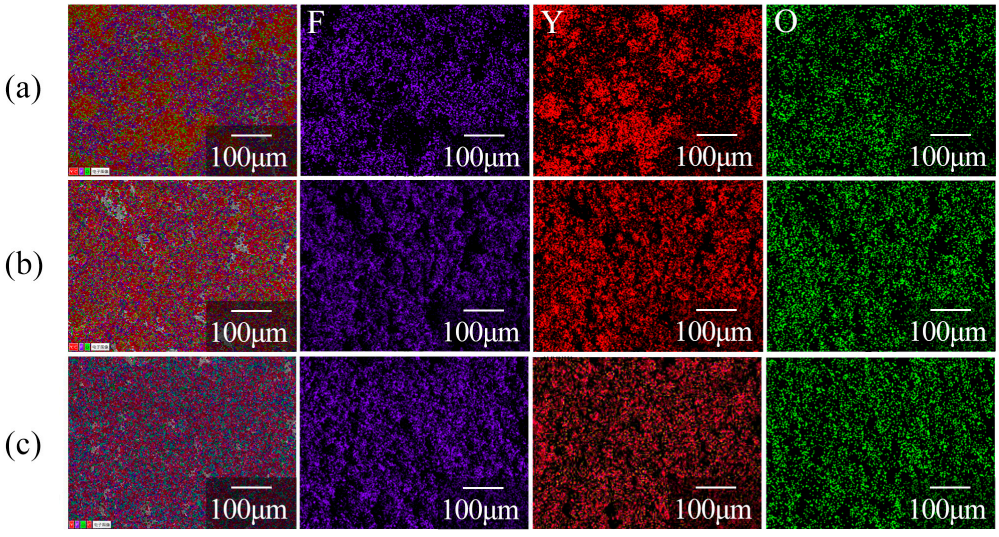

Figure 6. EDS maps of coating surfaces after CF_4/CHF_3 etching: (**a**) APS; (**b**) LAPS+500W; (**c**) LAPS+600W.

3.3. CF_4/CHF_3 Plasma Etching Behavior

Figure 7 shows the etching rates of the three coatings. The etching rates of the APS, LAPS+500W and LAPS+600W coatings were 1.675 mg/dm^2, 1.175 mg/dm^2 and 1.8 mg/dm^2. The LAPS+500W coating showed the lowest etching rate, with a mass loss of 70.15% and 65.28% relative to the APS and the LAPS+600W coatings, respectively. As evidenced in Table 3, the LAPS+500W coating exhibited the least reduction in thickness, while the LAPS+600W coating demonstrated the most significant reduction. This was consistent with the etching rates of the three coatings, indicating that the LAPS+500W coating had the best etching resistance.

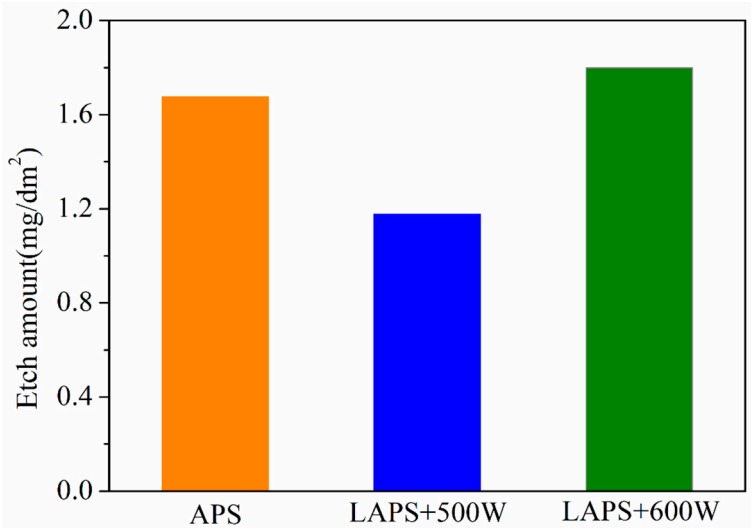

Figure 7. Etch amount of LAPS-Y_2O_3 coatings by CF_4/CHF_3 plasma etching.

Table 3. Thickness of three coatings before and after plasma etching.

	APS	LAPS+500W	LAPS+600W
Before (μm)	474.494	425.914	452.874
After (μm)	448.485	415.463	414.96
Decrease ratio	5.48%	2.45%	8.37%

Figure 8 shows the test results for the chemical composition alterations of the APS, LAPS+500W and LAPS+600W coatings after CF_4/CHF_3 etching (73.4 h) with varying XPS etching times (0–200 s). The alteration of the elements could be roughly divided into two distinct stages. The first stage, from the surface coating to the etching using XPS for around 50 s, the atomic concentration in this area changed dramatically; the fluorine and yttrium increased while the carbon and oxygen decreased. The fluorine content of the APS, LAPS+500W and LAPS+600W coatings increased from 33.66, 40.5 and 24.32 atomic% to 48.76, 60.15 and 49.76 atomic%, respectively. These values increased by 44.9%, 48.5% and 104.6%, respectively. In this stage, the coating underwent a transition from a carbon polymer layer to a fluorination layer [10]. In the second stage, XPS etching for 50 s to XPS etching for 200 s, the changes in the atomic concentration tended to be flat, and the fluorine concentration of the three coatings increased by 10.9%, 1.65% and 3.88%, respectively. The concentration of the LAPS+500W coating changed the least during this stage, indicating that the composition of the coating was the most stable. Since the powder did not contain carbon, the carbon in the sample had primarily randomly infiltrated from the atmospheric environment during the preparation of the coating. As the etching progressed, some of the carbon combined with oxygen evaporated into a vapor phase (COz), while some remained on the coating in the form of a polymer.

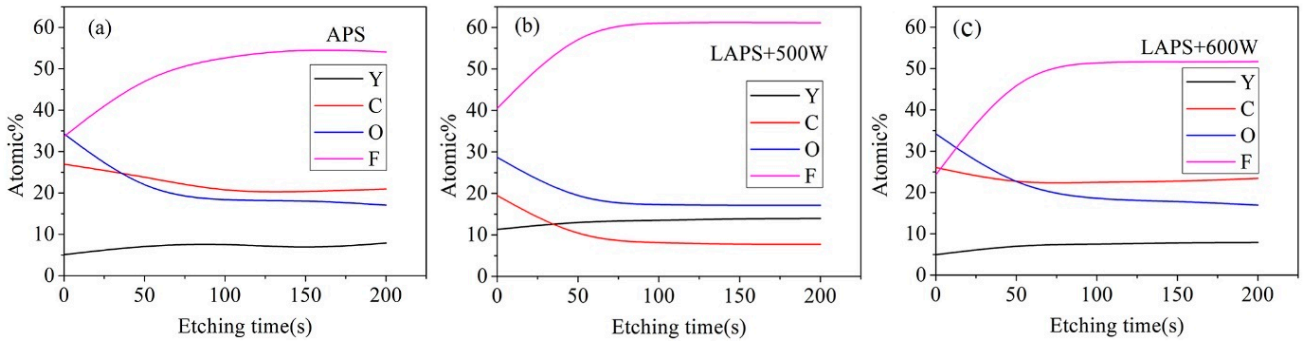

Figure 8. Variations in chemical compositions measured by XPS after CF_4/CHF_3 plasma etching: (**a**) APS; (**b**) LAPS+500W; (**c**) LAPS+600W.

Figure 9 shows the position of the spectral peaks of the three coatings after XPS etching for 200 S. The chemical compositions of the APS and LAPS+600W coatings were similar. The carbonate peaks (C1s) at 286.7 (APS) and 286.78 (LAPS+600W) eV and the Y-OH peaks (O1s) at 531.93 (APS) and 531.85 (LAPS+600W) eV indicated the presence of carbonate bonds in the coatings, which was similar to the findings of another report [20]. Furthermore, they confirmed the polymer morphology of the carbon described above.

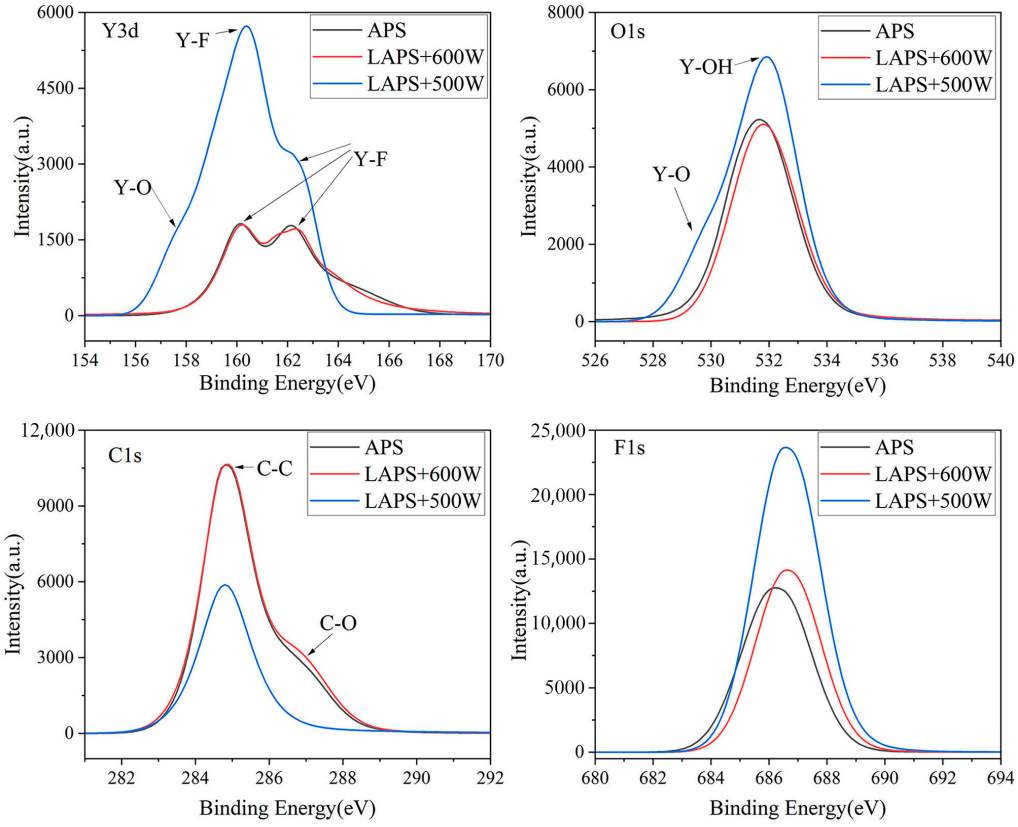

Figure 9. Narrow scans of XPS after CF_4/CHF_3 plasma etching of three coatings.

Two strong peaks with a higher binding energy (162.13 and 160.29 eV for APS and 162.05 and 160.09 eV for LAPS+600W) and two relatively weak peaks (159.56 and 158.83 eV for APS and 158.15 and 157.44 eV for LAPS+600W) were identified in the yttrium spectrum. The strong peaks were identified as Y-F bonds, and the weak peaks were determined to be Y-O bonds. Since the electronegativity of fluorine (4.0) is higher than that of oxygen (3.5), the binding energy of the Y-F bond formed when fluorine replaces oxygen is higher than that of the Y-O bond [28]. However, the peaks of the Y-O bonds in the spectra of

the APS and APS+600W coatings were not discernible in the yttrium spectrum shown in Figure 9, because they were too weak to show up in the image. The peak intensity ratios of the Y-F and Y-O bonds obtained from the XPS spectra of yttrium in the APS and LAPS+600W coatings were 8.4:1 (APS) and 78:1 (LAPS+600W), which were much higher than the average ratio (2.2) [29]. The weak peaks of the Y-O bond in O1s (530.59 eV for APS and 530.32 eV for LAPS+600W) were in accordance with this result. The spectral peaks of Y3d and O1s showed that the Y-O bonds had been eroded or replaced by Y-F bonds, indicating that the coatings had been severely corroded, especially the LAPS+600W coating.

In contrast, there was no significant carbonate peak (C1s) in the LAPS+500W coating, which was consistent with the low content of the C element in the coating in Figure 7. In addition to the Y-OH (532.0 eV) bond, an evident Y-O bond (529.96 eV) was observed in the O1s spectrum of the LAPS+500W coating, which was verified by the Y3d3/2 peak (159.18 eV) and Y3d5/2 peak (157.72 eV) in the Y3d spectrum. Furthermore, the peak of Y3d of the LAPS+500W coating was the strongest, and the peak intensity ratios of the Y-F bonds in the three coatings were 1 (APS):1.3 (LAPS+500W):1.1 (LAPS+600W).

Figure 10 shows the XPS spectra of yttrium at the LAPS+500W coating surface, etched for 50 s and etched for 200 s (etching for 50 s was chosen because this was close to the atomic concentration change turning point). Figure 10a shows the spectral peaks of the yttrium element at three etching depths, which intuitively shows how the intensity of the Y3d peak changed with depth. Figure 10b–d represent the narrow spectrum of the Y3d peaks at the surface, etched for 50 s and etched for 200 s. The intensity ratios of Y-F peaks from the top to the bottom were 1:1.18:1.15. The intensity ratios of the Y-F peaks and Y-O peaks at each position were 2.33 (surface), 2.35 (etched for 50 s) and 1.88 (etched for 200 s), and the first two ratios were close to the ratio (2.2) obtained by Cao et al. on the coating surface [29]. It can be seen from Figure 10 that the Y3d peaks at the three positions exhibited a shift, which was primarily attributed to fluoridation [11]. The intensity of the Y-O bond increased with depth, indicating that the effects of etching began to diminish.

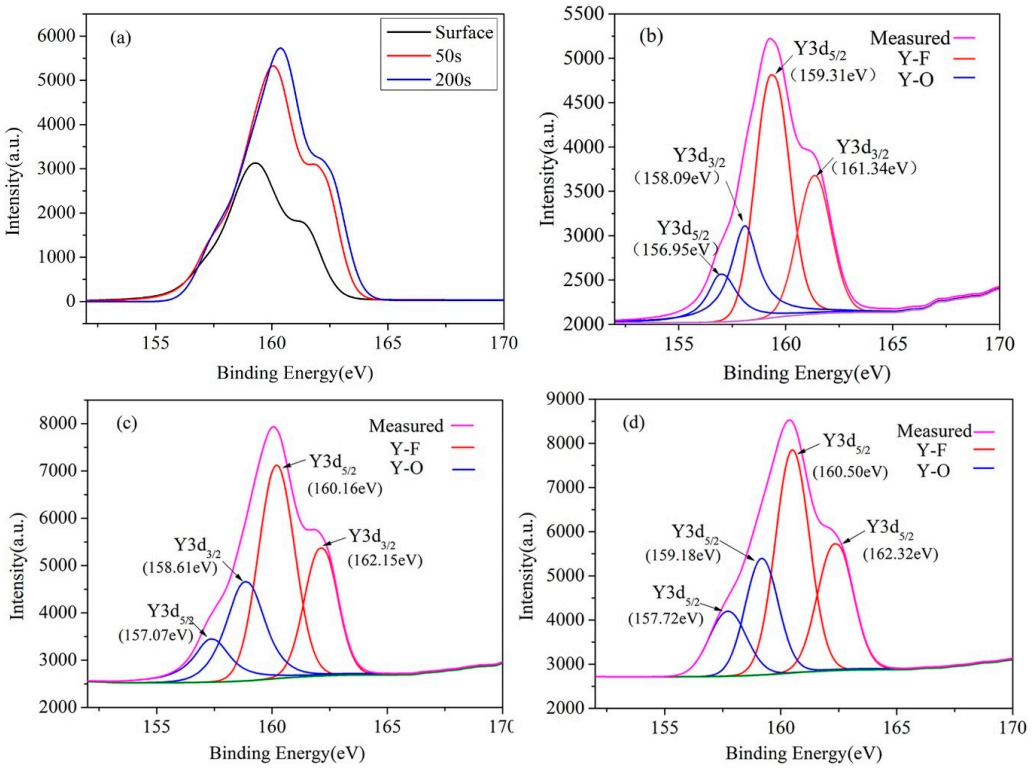

Figure 10. Peak positions of the XPS spectra of LAPS+500W coating. (**a**) Spectral peaks of yttrium. Narrow spectrum of yttrium on the (**b**) surface, (**c**) after 50 s of etching, and (**d**) after 200 s of etching.

In order to elucidate the phenomenon of the three coatings, the etching process should be taken into consideration. The entire etching process was divided into four distinct steps. First step: the CF_4/CHF_3 gas underwent a complex dissociation reaction during electron impact, resulting in the formation of dozens of reactants, including F^+, CF^+, $CF_2{}^+$, $CF_3{}^+$, and CHF^+ [30]. Second step: the ionized free radicals were deposited on the coating surface to form a layer of fluorocarbon film. Third step: the deposited free radicals reacted with the surface to decompose the Y-O bond and form a YO_xF_y layer. Fourth step: the coating was removed, and a reaction gradient was established by means of physical impact and chemical degradation [31,32].

In the second step, fluorine-free radicals deposited on the surface of the coating would diffuse. The diffusion of fluorine was affected by defects, temperature, density, etc. J. Kirchhof et al. found that a high hydroxyl concentration could potentially increase the diffusion rate of fluorine [33]. Due to the lower density caused by more defects, the fluorine concentrations of the APS and LAPS+600W coatings were lower than that of the LAPS+500W coating. In addition, it could be seen from the peaks of O1s in Figure 9 that the LAPS+500W coating had a higher hydroxyl concentration. Therefore, the fluorine diffused rapidly on the LAPS+500W coating, which could facilitate the formation of the fluorination layer faster in the third step. The formation of the fluorination layer can play a certain role in protecting the coating.

The results of the SEM and EDS in Figure 11 support the conclusion above. There were some dark regions at the edge of the coating in the SEM images (shown by the yellow arrows in the figure). According to the EDS maps, it could be determined that these regions belong to the fluorination layer. Compared with the other two coatings, the fluorination layer of the LAPS+500W coating was wider and thicker. However, in the regions composed of defects (shown by the red circles in the figure), the concentration of the yttrium and fluorine elements decreased, whereas that of the carbon element exhibited an increase. Meanwhile, the content of the yttrium element around the defects also decreased. This indicated that the coating at the defects had undergone serious erosion, and this erosion behavior tended to spread. This phenomenon can be explained by the cohesive force of the coating. As mentioned above, the defects in the coatings were mainly pores, and the pores were mostly caused by the presence of unmelted particles which were mainly mechanically bonded. On the contrary, the dense area of the coating was dominated by metallurgical bonding and the binding force was higher than that in a mechanically bonded coating. Therefore, the defect regions were more susceptible to erosion during plasma etching. In addition, the presence of carbon within the defects of the coating was identified (illustrated by the yellow circles in the figure), which had penetrated into the coating during the preparation process.

In the third stage, the formation process of the fluorination layer could be expressed as follows:

$$Y_2O_3(s) + aCF_m(g) \rightarrow YO_xF_y\ (s) + bCO_z\ (g),$$

YO_xF_y is a non-stoichiometric compound and YF_x is the ideal form. During the formation of YO_xF_y, some Y-O bonds were replaced by Y-F bonds with higher energy, resulting in volume expansion and stress generation. Accordingly, the YO_xF_y layer was more easily removed by physical sputtering rather than chemical reactions [20,32]. Since physical sputtering and chemical degradation occur simultaneously in the plasma etching process, the etching process of the yttrium oxide coating could be performed as depicted in Figure 12.

According to the results of the SEM, EDS and XPS analyses, combined with the etching rates of the three coatings, we believed that the density was the primary factor influencing the differing etching resistance of the three coatings. The APS and LAPS+600W coatings were seriously eroded due to the presence of numerous defects, and the low yttrium content and weak Y-O bonds in the surface area indicated that the fluorination layer was rapidly eroded.

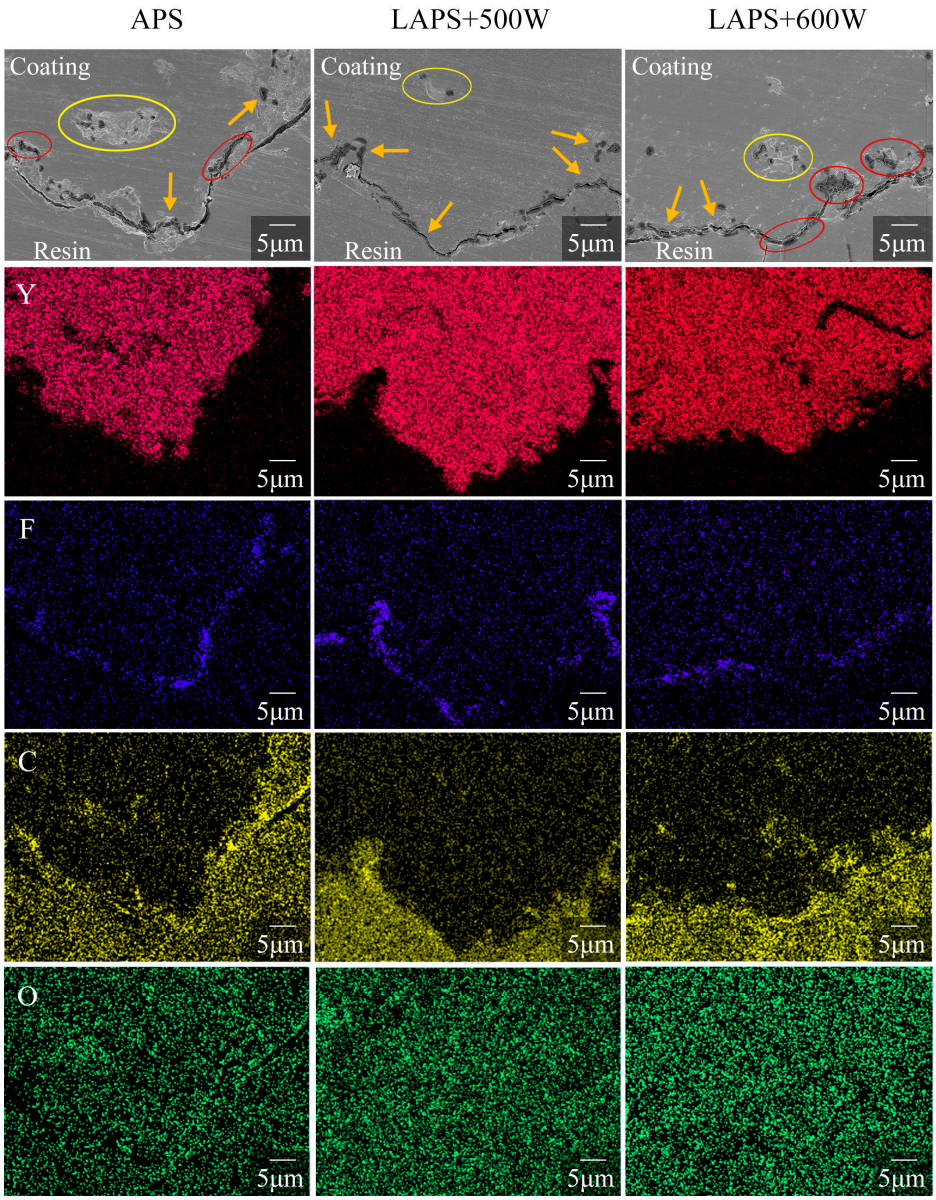

Figure 11. FE-SEM images and EDS maps of coating after CF_4/CHF_3 etching.

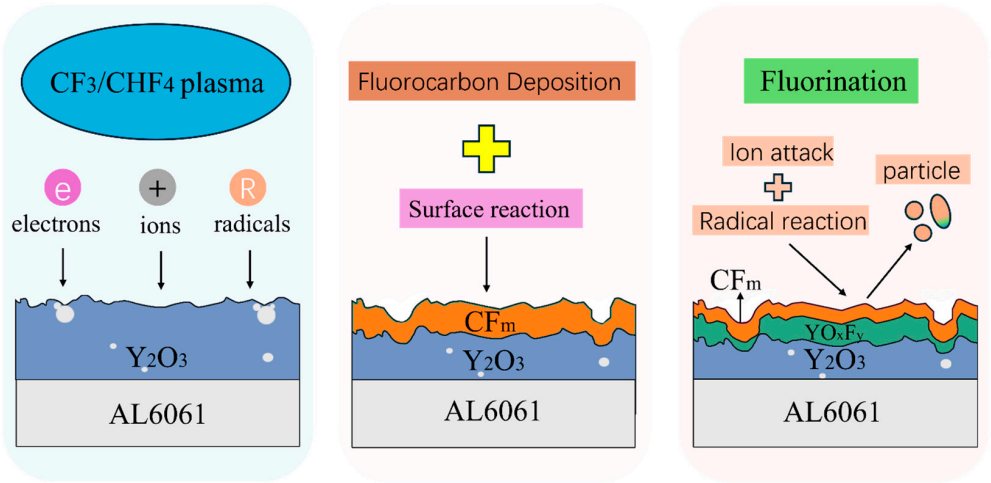

Figure 12. Deposition and etching behavior of Y_2O_3-coated yttrium oxyfluoride thin films.

4. Conclusions

In this study, yttrium oxide coatings were prepared by atmospheric plasma spraying combined with different in situ laser irradiation powers. The results showed that laser coupling did not alter the phase composition of the coatings, but it enhanced the density and reduced the porosity. However, an excessive laser power (600 W) caused cracks. After coupling with a 500 W laser, more powder particles melted, which decreased the thickness and internal defects of the coating and increased the binding force. Owing to the high density, the LAPS+500W coating formed a thicker and wider fluorination layer after CF_4/CHF_3 plasma etching. In contrast, for the coating with more defects (APS and LAPS+600W), the defect areas were first eroded due to the low binding force of the particles, and the corrosion resistance of the adjacent areas was reduced. The findings demonstrated that the defects had a significant effect on the etching resistance of the coating and the laser coupled with atmospheric plasma spraying effectively reduced defects and enhanced the plasma etching resistance of the coating. Therefore, in situ laser-assisted plasma spraying is a promising method for producing high-quality yttrium oxide coatings.

Author Contributions: X.Z.: data curation, writing—original draft. J.Y.: project administration, writing—review and editing. T.X.: investigation, methodology. P.Z.: conceptualization. Z.Y.: writing—review and editing. Q.Z.: resources. J.D.: validation. Y.S.: methodology. All authors have read and agreed to the published version of the manuscript.

Funding: This research was funded by "Pioneer" and "Leading Goose" Research and Development Program of Zhejiang Province (2023C01052, 2024C01178), National Natural Science Foundation of China (52475313).

Institutional Review Board Statement: Not applicable.

Informed Consent Statement: Not applicable.

Data Availability Statement: The data are contained within the article.

Conflicts of Interest: Author Jiake Deng was employed by the company Wuhan HGLaser Engineering Co., Ltd. Author Yongfeng Sui was employed by the company Hangzhou Turbine Power Group Co., Ltd. The remaining authors declare that the research was conducted in the absence of any commercial or financial relationships that could be construed as a potential conflict of interest.

References

1. Coburn, J.W.; Winters, H.F. Plasma etching—A discussion of mechanisms. *J. Vac. Sci. Technol.* **1979**, *16*, 391–403. [CrossRef]
2. Donnelly, V.M.; Kornblit, A. Plasma etching: Yesterday, today, and tomorrow. *J. Vac. Sci. Technol.* **2013**, *31*, 050825. [CrossRef]
3. Kasashima, Y.; Nabeoka, N.; Motomura, T.; Uesugi, F. Many flaked particles caused by impulsive force of electric field stress and effect of electrostriction stress in mass-production plasma etching equipment. *Jpn. J. Appl. Phys.* **2014**, *53*, 040301. [CrossRef]
4. Ishimaru, H. Ultimate pressure of the order of 10–13 Torr in an aluminum alloy vacuum chamber. *J. Vac. Sci. Technol. A* **1989**, *7*, 2439–2442. [CrossRef]
5. Tezani, L.; Pessoa, R.; Maciel, H.; Petraconi, G. Chemistry studies of SF_6/CF_4, SF_6/O_2 and CF_4/O_2 gas phase during hollow cathode reactive ion etching plasma. *Vacuum* **2014**, *106*, 64–68. [CrossRef]
6. Song, J.-B.; Choi, E.; Oh, S.-G.; So, J.; Lee, S.-S.; Kim, J.-T.; Yun, J.-Y. Improved reliability of breakdown voltage measurement of yttrium oxide coatings by plasma spray. *Ceram. Int.* **2019**, *45*, 22169–22174. [CrossRef]
7. Guo, M.; Yang, L.; Li, P.Y.; Xu, Z.T.; Xu, C.Y.; Wang, Q.D.; Li, Y. Tribological Behavior Regulation of Graphene Nanocrystallites Embedded Carbon Film by Fluorine Plasma Etching. *J. Mech. Eng.* **2024**, *60*, 216–226.
8. Fukumoto, H.; Fujikake, I.; Takao, Y.; Eriguchi, K.; Ono, K. Plasma chemical behaviour of reactants and reaction products during inductively coupled CF_4plasma etching of SiO_2. *Plasma Sources Sci. Technol.* **2009**, *18*, 045027. [CrossRef]
9. Kim, D.-P.; Yeo, J.-W.; Kim, C.-I. Etching properties of Al_2O_3 films in inductively coupled plasma. *Thin Solid Films* **2004**, *459*, 122–126. [CrossRef]
10. Cao, Y.-C.; Zhao, L.; Luo, J.; Wang, K.; Zhang, B.-P.; Yokota, H.; Ito, Y.; Li, J.-F. Plasma etching behavior of Y_2O_3 ceramics: Comparative study with Al_2O_3. *Appl. Surf. Sci.* **2016**, *366*, 304–309. [CrossRef]
11. Kreethi, R.; Hwang, Y.-J.; Lee, H.-Y.; Park, J.-H.; Lee, K.-A. Stability and plasma etching behavior of yttrium-based coatings by air plasma spray process. *Surf. Coat. Technol.* **2023**, *454*, 129182. [CrossRef]
12. Lin, T.K.; Wang, W.K.; Huang, S.Y.; Tasi, C.T.; Wuu, D.S. Comparison of erosion behavior and particle contamination in mass-production CF_4/O_2 plasma chambers using Y_2O_3 and YF_3 protective coatings. *Nanomaterials* **2017**, *7*, 183. [CrossRef] [PubMed]

13. Song, J.B.; Kim, J.T.; Oh, S.G.; Yun, J.Y. Contamination Particles and Plasma Etching Behavior of Atmospheric Plasma Sprayed Y_2O_3 and YF_3 Coatings under NF_3 Plasma. *Coatings* **2019**, *9*, 102. [CrossRef]
14. Song, J.B.; Choi, E.; Oh, S.G.; Kim, J.T.; Yun, J.Y. Contamination Particle Behavior of Aerosol Deposited Y_2O_3 and YF_3 Coatings under NF_3 Plasma. *Coatings* **2019**, *9*, 310. [CrossRef]
15. Ma, T.; List, T.; Donnelly, V.M. Comparisons of NF3 plasma-cleaned Y_2O_3, YOF, and YF_3 chamber coatings during silicon etching in Cl_2 plasmas. *J. Vac. Sci. Technol. A* **2018**, *36*, 031305. [CrossRef]
16. Tan, Y.; Wang, Y.; Wu, S.; Chen, P.; Zhu, Z.; Tian, Z. Sputtering resistance and damage mechanism of Y_2O_3-based ceramics etching by Xe plasma. *Mater. Today Commun.* **2021**, *26*, 101775. [CrossRef]
17. Hwang, Y.J.; Kim, K.W.; Lee, H.Y.; Kwon, S.C.; Lee, K.A. Effect of Spray Angle the on Microstructure and Mechanical Prop-erties of Y_2O_3 Coating Layer Manufactured by Atmospheric Plasma Spray Process. *J Korean Powder Met. Inst.* **2021**, *28*, 310–316. [CrossRef]
18. Kassner, H.; Siegert, R.; Hathiramani, D.; Vassen, R.; Stoever, D. Application of suspension plasma spraying (SPS) for manu-facture of ceramic coatings. *J. Therm. Spray Technol.* **2008**, *17*, 115–123. [CrossRef]
19. Lee, S.J.; Lee, J.H.; Hwang, N.M. Yttrium Oxyfluoride Coating Deposited with a $Y_5O_4F_7/YF_3$ Suspension by Suspension Plasma Spraying Under Atmospheric Pressure. *J. Therm. Spray Technol.* **2022**, *31*, 1508–1520. [CrossRef]
20. Kim, M.J.; Choi, E.; Lee, D.G.; Seo, J.P.; Back, T.S.; So, J.H. The effect of powder particle size on the corrosion behavior of at-mospheric plasma spray-Y_2O_3 coating: Unraveling the corrosion mechanism by fluorine-based plasma. *Appl. Surf. Sci.* **2022**, *606*, 154958. [CrossRef]
21. Dubourg, L.; Lima, R.; Moreau, C. Properties of alumina–titania coatings prepared by laser-assisted air plasma spraying. *Surf. Coat. Technol.* **2007**, *201*, 6278–6284. [CrossRef]
22. Zhou, Y.; Xu, L.F.; Zheng, H.Z.; Wang, D.S. Surface modification of plasma spraying Al_2O_3-13 wt% TiO_2 coating by laser remelting technique. *Mater. Res. Express* **2022**, *9*, 056401. [CrossRef]
23. Kai, C.; Yong, Z.; Dongting, W.; Yingwen, T.; Yongang, Z. Pulsed laser remelting supersonic plasma sprayed Cr_3C_2-NiCr coatings for regulating microstructure hardness and corrosion properties. *Surf. Coat. Technol.* **2021**, *418*, 127258.
24. Janka, L.; Norpoth, J.; Eicher, S.; Ripoll, M.R.; Vuoristo, P. Improving the toughness of thermally sprayed Cr_3C_2-NiCr hardmetal coatings by laser post-treatment. *Mater. Des.* **2016**, *98*, 135–142. [CrossRef]
25. Zhang, P.P.; Jiang, S.Y.; Guo, Y.J.; Sui, Y.F.; Ding, X.Y.; Yao, Z.H. Microstructures and Wear Resistance of Mo Coating Fabri-cated by In Situ Laser-Assisted Plasma Spraying. *J. Therm. Spray Technol.* **2023**, *33*, 233–245. [CrossRef]
26. Li, J.J.; Zhang, Y.F.; Li, Q.; Ran, X.; Hao, Q.; Guo, X.L. Influence of atmospheric plasma spraying process parameters on microstructure and properties of yttrium oxide coatings. *Dig. J. Nanomater. Biostr.* **2024**, *19*, 1–13. [CrossRef]
27. Zhou, Z.; Zhang, L.; Dong, X.Y.; Luo, X.T.; Mahrukh, M.; Li, C.J. Mechanism of Suppressing Oxidation of FeAl Molten Droplet by Adding C to Powder and Its Effect on Microstructure and Properties of Plasma-sprayed Coating. *China Surf. Eng.* **2023**, *36*, 44–56.
28. Gadow, R.; Killinger, A.; Stiegler, N. Hydroxyapatite coatings for biomedical applications deposited by different thermal spray techniques. *Surf. Coat. Technol.* **2010**, *205*, 1157–1164. [CrossRef]
29. Tillmann, W.; Khalil, O.; Abdulgader, M. Porosity Characterization and Its Effect on Thermal Properties of APS-Sprayed Alumina Coatings. *Coatings* **2019**, *9*, 601. [CrossRef]
30. Vickerman, J.C.; Gilmore, I.S. *Surface Analysis*, 2nd ed.; Wiley: New York, NY, USA, 2009; p. 53.
31. Kim, B.H.; Kwon, S.K. Oxide via etching in a magnetically enhanced $CHF_3/CF_4/Ar$ plasma. *Solid-State Electron.* **2003**, *47*, 1799–1803. [CrossRef]
32. Moritz, K.; Moritz, L.; Weber, M.S.; Rahel, B.; Egbert, W.; Martin, B. The role of fluorination during the physicochemical erosion of yttria in fluorine- based etching plasmas. *J. Eur. Ceram. Soc.* **2022**, *42*, 561–566.
33. Kirchhof, J.; Unger, S.; Klein, K.F.; Knappe, B. Diffusion behaviour of fluorine in silica glass. *J. Non-Cryst. Solids* **1995**, *181*, 266–273. [CrossRef]